NEW CARBON MATERIALS
Volume 32, Issue 6, Dec. 2017
Online English edition of the Chinese language journal

Available online at www.sciencedirect.com
ScienceDirect

Cite this article as: New Carbon Materials, 2017, 32(6): 509-516

RESEARCH PAPER

SAPO-34 templated growth of hierarchical porous graphene cages as electrocatalysts for both oxygen reduction and evolution

Ling Zhong, Cheng Tang, Bin Wang, Hao-Fan Wang, Shang Gao, Yao Wang*, Qiang Zhang*

Beijing Key Laboratory of Green Chemical Reaction Engineering and Technology, Department of Chemical Engineering, Tsinghua University, Beijing 100084, China

Abstract: Three-dimensional hierarchical porous graphene materials with unique properties are of significant importance for the exploration of advanced electrocatalysts for both the oxygen reduction and evolution reactions (ORR/OER). Templated chemical vapor deposition is a favorable strategy to fabricate this kind of graphene, but the number of effective templates is limited. Here, silicoaluminophosphate (SAPO-34) zeolite crystals were used as the catalytic templates for the deposition of hierarchical porous graphene. The graphene obtained consisted of micron-size hollow cubes with mesoporous/nanoporous facets, and ultrathin walls, precisely replicating the structure of the cube-like SAPO-34 zeolite particles. A high doping level of nitrogen (6.84 at%) was achieved by subsequent annealing at 700 °C under ammonia before template removal. Because of the unique porosity, abundant defects, and favorable N-doping, the N-doped graphene exhibited considerable reactivity for both ORR and OER.

Key Words: Graphene materials; Hierarchical pore structure; Oxygen reduction; Oxygen evolution; Zeolite; SAPO-34; Nitrogen doping nanocarbon.

1 Introduction

Energy electrocatalysis, including oxygen reduction reaction (ORR) and oxygen evolution reaction (OER), is attracting increasing attention during the past decade, which is the kernel and bottleneck of future energy technologies, such as metal-air batteries, fuel cells and water splitting [1-4]. However, these electrocatalytic reactions are always kinetically sluggish due to the multi-step proton-coupled electron transfer and triple-phase boundary regions, thereby leading to urgent requirements of effective electrocatalysis [5]. Generally, precious-metal-based materials can serve as the benchmark electrocatalysts, such as Pt/C for ORR, and IrO_2/RuO_2 for OER [6, 7]. Nevertheless, the scarce reserves and high cost of these benchmark electrocatalysts limit the large-scale promotion and commercialization. Up to date, various alternatives have been developed to replace the precious-metal-based electrocatalysts with comparable activity and durability, such as transition-metal oxides/sulfides/hydroxides/hydroxysulfides [8, 9], nanocarbon materials [10-13], and their hybrids [14, 15]. Among them, the nanocarbon materials have been widely demonstrated to play a pivotal and versatile role in energy electrocatalysis, which can serve as multifunctional substrates or provide highly active sites for superb electrocatalytic performances [16, 17]. The reactivity greatly depends on the appropriate nanostructures and functionalities of employed nanocarbon materials, including the size, hierarchical porosity, electrical conductivity, heteroatom doping, functional groups, et al[18-20].

Specifically, the three-dimensional (3D) hierarchical porous graphene (hpG) affords an attractive platform for the development of the advanced electrocatalysts, benefited from the high conductivity, large surface area, 3D interconnected porosity, facilely tunable surface chemistry, and cost-effective fabrication. In general, 3D hpG materials are dominantly fabricated *via* sol-gel self-assembly of graphene oxides [21] or chemical vapor deposition (CVD) growth on templates (*e.g.* porous Ni [22], mesoporous MgO [14], porous CaO [23], layered double oxides [24], et al.). Compared with the sol-gel strategy, the templated growth is more favorable to regulate the porous hierarchy with a high conductivity, and modify the intrinsic activity by *in-situ* doping. Mesoporous graphene frameworks fabricated using mesoporous MgO templates have been reported as excellent metal-free catalysts for ORR/OER or multifunctional substrates for hybrid catalysts [10, 14]. In addition to the catalytic substrates for graphene deposition, some nanoporous templates can also serve as nano-reactors to fabricate emerging hybrid catalysts, such as monodisperse Pt

Received date: 10 Sep 2017; **Revised date:** 9 Oct 2017
***Corresponding author.** E-mail: wang_yao@mail.tsinghua.edu.cn; zhang-qiang@ mails. tsinghua. edu. cn

DOI: 10.1016/S1872-5805(17)60136-7

nanoparticles confined in graphene nanobox constructed on zeolite A [25]. However, only few kinds of effective templates for the fabrication of hpG materials were reported, limiting the feasibility to adjust the resultant morphologies and functionalities. Besides, the understanding of the graphene growth behavior on these templates, especially the porous metal oxides, is still preliminary. Consequently, there is a plenty of space to engineer the 3D hpG materials with new templates and strategies for a bright application in energy electrocatalysis and other fields.

In this contribution, we report a family of 3D hierarchical porous graphene cages (hpGCs) fabricated *via* CVD on SAPO-34 templates, which affords promising applications in energy electrocatalysis. As-obtained hpGC materials exhibit microsized hollow cubes with mesoporous/nanoporous facets, precisely replicating the morphology of SAPO-34 templates. Besides, the graphene is less than three layers due to the catalytic effect of the outer acidic surfaces of SAPO-34. Nitrogen heteroatoms can be facilely incorporated into the framework with a high content (the sample is denoted as N-hpGC) by the introduction of ammonia during CVD synthesis. Attributed to the abundant topological defects in such nanostructure and favorable nitrogen doping, such hpG materials are revealed to be active for both ORR and OER electrocatalysis.

2 Experimental

2.1 Material synthesis

The SAPO-34 zeolites were fabricated by a routine hydrothermal method as described in previous reports [26]. The hpGC was synthesized via CVD method with as-obtained SAPO-34 as templates and methane as carbon source. SAPO-34 templates were dispersed uniformly on a quartz boat which was placed in the center of a horizontal quartz tube at atmospheric pressure. The tube was then inserted into a furnace. The reactor was heated to 950 ^{o}C under flowing Ar (200 mL min^{-1}), and then methane (60 mL min^{-1}) was simultaneously introduced into the reactor for 5 min. The furnace was then cooled to 700 ^{o}C, and ammonia (60 mL min^{-1}) was introduced for 2.0 h for the synthesis of N-hpGC. Afterwards, the furnace was cooled to room temperature under Ar protection. As-obtained products (denoted as SAPO-34@hpGC and SAPO-34@N-hpGC) were purified by HF to remove the SAPO-34 templates. After treatments with washing, filtering, and freeze-drying, hpGC and N-hpGC were obtained.

2.2 Characterizations

The morphology and structure of the samples were characterized using a JSM 7401F (JEOL Ltd., Tokyo, Japan) scanning electron microscope (SEM) operated at 3.0 kV and a JEM 2010 (JEOL Ltd., Tokyo, Japan) transmission electron microscope (TEM) operated at 120.0 kV. X-ray diffraction (XRD) patterns were recorded on a Bruker D8 Advance diffractometer at 40.0 kV and 120 mA with Cu-*K*α radiation. X-ray photoelectron spectroscopy (XPS) measurements were carried out by a Escalab 250xi. Raman spectra were obtained using a Horiba Jobin Yvon LabRAM HR800 Raman spectrophotometer with a He–Ne laser excitation at 633 nm.

2.3 Electrocatalytic performance evaluation

All electrochemical measurements were performed in a three-electrode system (CHI 760D, CH Instrument, USA), using Pt sheet as a counter electrode and saturated calomel electrode (SCE) as a reference electrode.

The fabrication of working electrode was carried out as follows: 5.0 mg catalyst was firstly dispersed in 0.95 mL ethanol, then 0.05 mL Nafion solution (5.0 wt%) was introduced, followed by 1.0 h sonication to form a relatively homogeneous suspension. 10.0 μL of the suspension was pipetted onto the glassy-carbon disk electrode, which was mechanically polished and ultrasonically washed in advance. After solvent evaporation for 10.0 min in air, the working electrode was prepared for electrochemical measurements.

Rotating ring-disk electrode (RRDE) measurements for ORR were conducted on a RRDE configuration (Pine Research Instrument, USA) with a disk electrode (glassy carbon, diameter: 5.0 mm) and a ring electrode (Pt electrode, inner diameter: 6.5 mm, outer diameter: 7.5 mm). Linear sweep voltammetry (LSV) for OER was performed at a scan rate of 10.0 mV s^{-1} and a rotating rate of 1600 rpm on a rotating disk electrode (RDE) with a disk diameter of 5.0 mm in an O_2- saturated 0.10 M KOH solution. The electron transfer number n was calculated based on the disk (I_d) and ring current (I_r) as follows: $n = 4I_d/(I_d+I_r/N)$, where N is the current collection efficiency of the Pt ring (0.26). The overpotential was calculated by the following equation: Overpotential = measured value (*vs.* SCE) + 0.241 + 0.0592pH - 1.229 (*vs.* RHE). All polarization curves were corrected with 95% *iR*-compensation. The mass loading was *ca.* 0.25 mg cm^{-2} for all electrochemical measurements in this contribution.

3 Results and discussion

3.1 Templated CVD growth of hpGC on SAPO-34

SAPO-34 zeolite is an industrial catalyst for methanol-to-olefin conversion owing to the excellent shape selectivity, moderate acidity, and superior thermal and hydrothermal stability [27]. The framework structure possesses large CHA-type cages (0.94 nm in diameter) and narrow 8-ring pore (0.38 nm) openings. Because of the appropriate surface acidity and small-sized openings, the methane molecules are supposed to be predominately adsorbed on the crystal surface and catalytically transformed into few-layered graphene. Therefore, the SAPO-34 is expected to be a promising template for the deposition of hpGC materials.

The SEM image in Fig. 1a exhibits that as-synthesized SAPO-34 illustrates solid cube-like particles with a size of several micrometers. The facets are smooth with some porous

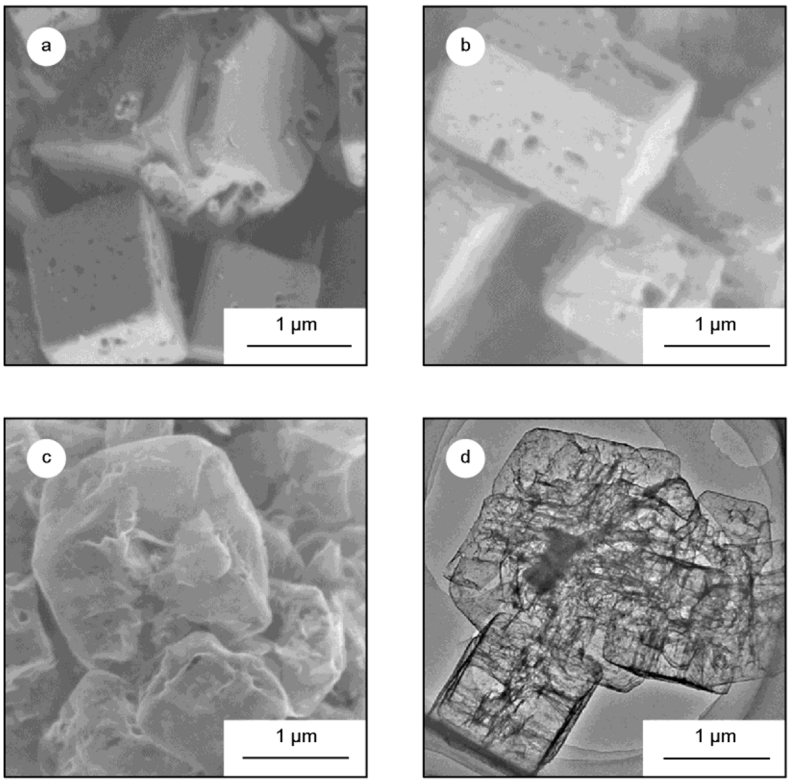

Fig. 1 Morphology of SAPO-34 molecular sieve template and as-obtained graphene materials. SEM images of (a) SAPO-34, (b) SAPO-34@hpGC, and (c) purified hpGC. (d) TEM image of purified hpGC.

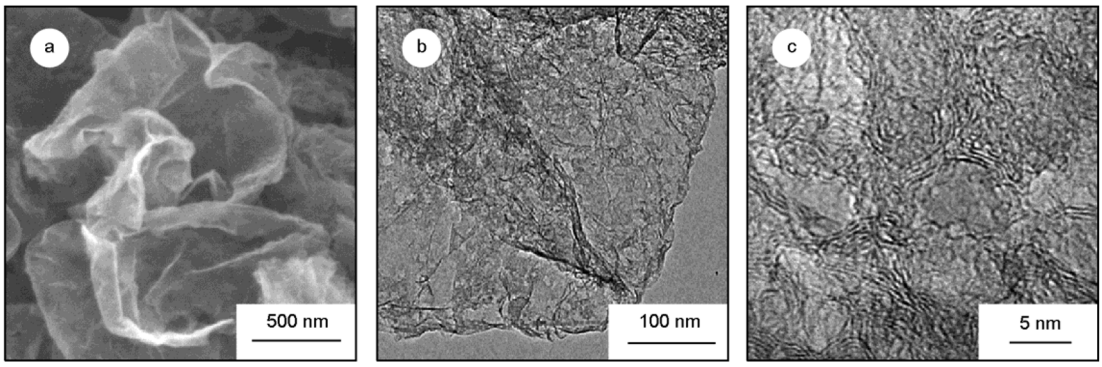

Fig. 2 Structure of hpGC materials. (a) SEM image and (b, c) TEM images of as-obtained hpGC,showing the porous and thin graphene layer.

openings or breakages which may be formed during the synthesis. During the methane CVD at 950°C for 5 min, the SAPO-34 preserves the structure and a thin layer of graphene is uniformly grown on the surfaces as shown in Fig. 1b. After the removal of the template by HF, 3D hpGC is successfully obtained with a hollow cage structure as confirmed by both SEM and TEM images (Fig. 1c and 1d). Remarkably, the graphene cages totally cover the surface of the SAPO-34 crystal, even replicating the surface steps (Fig. 1c), and form a continuous cage, revealing that the graphene growth is controlled by surface catalysis.

Fig. 2a shows a typical SEM image of hpGC with a collapsed structure. It is due to the mechanical imbalance between the ultrathin graphene and the large size hollow cages. Furthermore, the TEM image in Fig. 2b not only confirms that the graphene is ultrathin with a nearly transparent appearance under electron beams, but also clearly indicates that the graphene is integrated and continuous at the cube corner with three connected edges. Besides, the graphene layer is full of mesopores (Fig. 2b and 2c). This morphology has been widely reported in the graphene deposited on metal oxide templates [14, 23, 28], which may be related to the surface defects and unevenness of metal oxides that are different from metal substrates. The graphitic rings around mesopores are less than three layers, further revealing the high graphitic degree and ultrathin thickness (Fig. 2c).

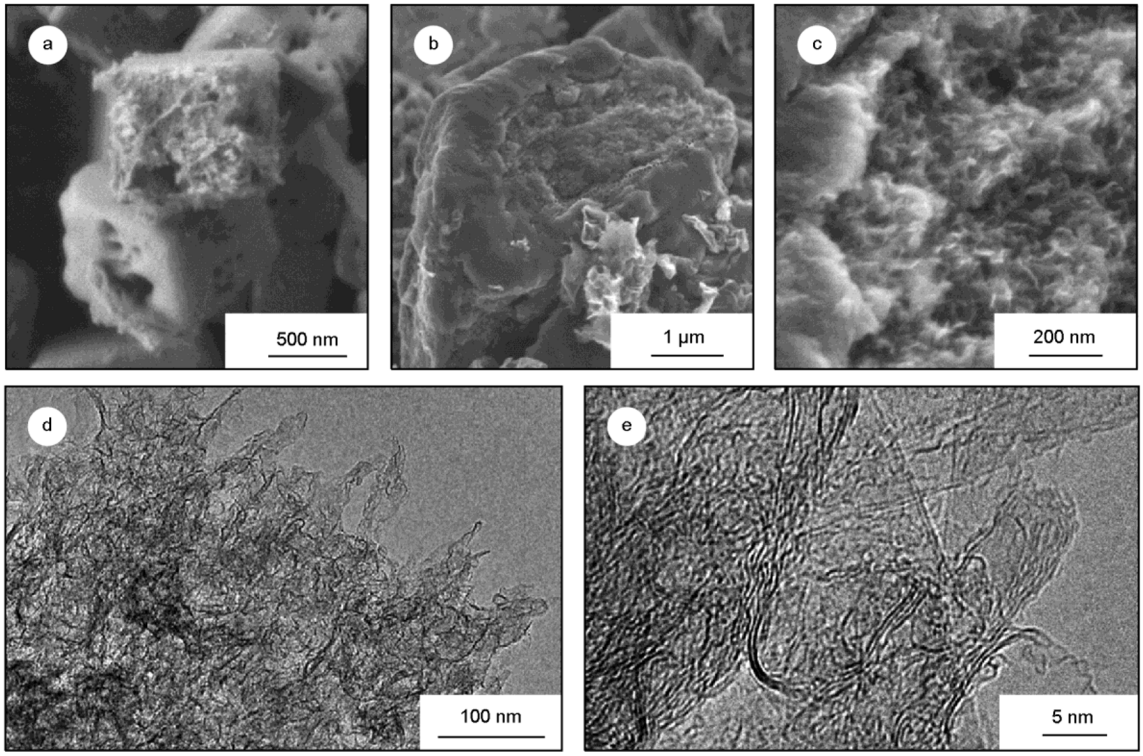

Fig. 3 The nanostructure of graphene materials grown on the SAPO-34 template. (a) SEM image of SAPO-34 with damaged facets. (b) SEM image and (c) high-resolution SEM image of as-obtained hpGC. (d) TEM image and (e) high-resolution TEM image of as-obtained hpGC.

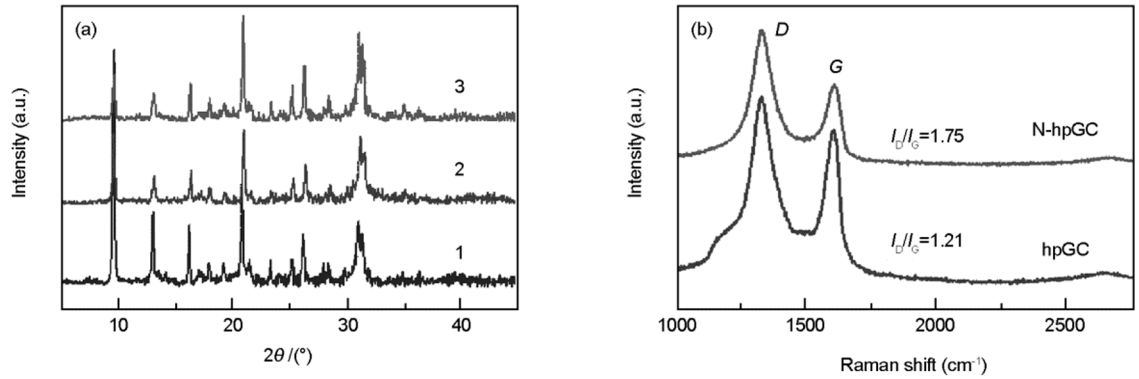

Fig. 4 Characterization of molecular sieve template and hpGC based materials. (a) XRD patterns of the synthesized SAPO-34 (line 1), SAPO-34@hpGC (line 2), and SAPO-34@N-hpGC (line 3) samples. (b) Raman spectra of hpGC and N-hpGC.

In some cases, the SAPO-34 particles are fragmented with some surfaces damaged, as shown in Fig. 3a. In contrast to the smooth surface, the damaged part exposes a large number of SAPO-34 fragments, which are also active to catalyze the graphene deposition. As a result, a continuous graphene layer can be obtained on the smooth part, while blanket-like graphene nanosheets are formed on the damaged part (Fig. 3b and 3c). The TEM image in Fig. 3d further reveals the presence of nano-sized graphene sheets, assembling into a structure obviously distinct from that in Fig. 2b. These graphene nanosheets are also ultrathin with a thickness less than three layers.

The above morphology characterizations indicate that the SAPO-34 is an effective substrate for the CVD growth of graphene with an ultrathin thickness and tunable porosity. The graphene deposition is self-limited on the surface of SAPO-34 crystals, whether the surfaces are smooth or fragmented. The replication of SAPO-34 structures leads to a micro-sized hollow cube, while the catalytic growth on uneven or fragmented surfaces results in a large number of mesopores and even nanopores in graphene. Therefore, the methane CVD on the SAPO-34 templates is demonstrated to facilely construct a hierarchical porous graphene structure, which is attractive for the application in energy fields.

3.2 Nitrogen doping of hpGC on SAPO-34

Nitrogen doping is the first revealed and the most researched strategy to provide high ORR and OER activities for metal-free nanocarbon materials [29]. The nitrogen heteroatoms can effectively change the charge distribution on

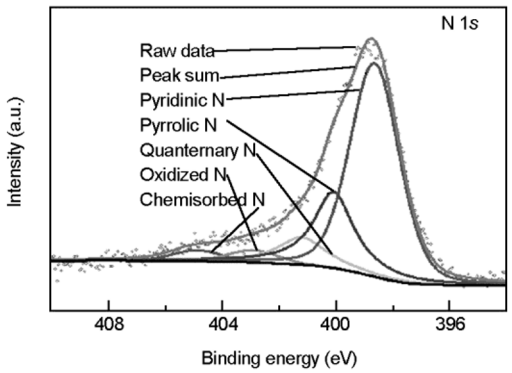

Fig. 5 The high-resolution N 1*s* XPS spectrum of N-hpGC.

the sp^2-conjugated carbon matrix, optimize the adsorption energy of intermediates and enhance the catalytic activity [30-32]. Therefore, we further conduct the nitrogen doping in hpGC by simply annealing the sample under ammonia atmosphere. As the ammonia can be chemisorbed on the acidic sites of SAPO-34 particles and significantly affect the growth of graphene on the surface, the ammonia was introduced after the graphene deposition had been finished.

Fig. 4a exhibits the XRD patterns of the pristine SAPO-34 particles, and those with graphene or nitrogen-doped graphene as deposited. There is no difference between them, revealing the excellent thermal and chemical stability of SAPO-34 templates at high temperature, and under the atmosphere of methane/ammonia. As-obtained N-hpGC sample is revealed to exhibit the similar morphology to the hpGC. It is interesting that the hierarchical porous graphene with a high graphitic degree and ultrathin thickness can be facilely fabricated on both acidic zeolites (such as SAPO-34 and zeolite A) and alkaline metal oxides (such as MgO and CaO). It is worthy to be further investigated to understand the growth behavior of graphene on substrates with different acidities. Notably, the acidity of SAPO-34 can be readily adjusted by tuning the Si/Al ratio, thereby providing a promising platform for the mechanism investigation.

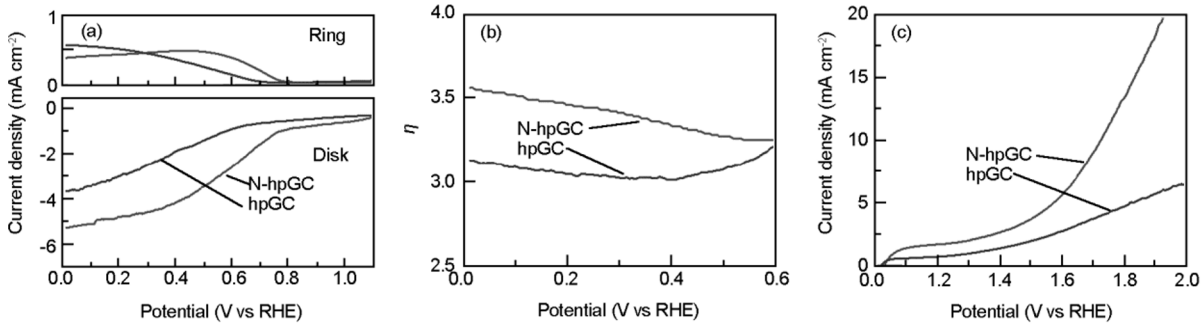

Fig. 6 ORR performance on graphene based electrocatalyst. (a) The disk current densities (bottom) and ring current densities (top) for ORR recorded on an RRDE. (b) Electron transfer number (**n**) derived from the LSV curves in RRDE measurements. (c) LSV curves for OER recorded on an RDE.

Raman spectra of the hpGC and N-hpGC were collected and presented in Fig. 4b, exhibiting two characteristic bands (*D* band corresponding to the phonon scattering at defect sites, and *G* band assigned to the in-plane vibration of sp^2 carbon). The I_D/I_G ratio of the N-hpGC (1.75) is revealed to be much higher than that of the hpGC (1.21), suggesting a relatively higher density of defects in the N-hpGC than the hpGC due to nitrogen doping. XPS survey spectrum reveals a high N content around 6.84 at% for the N-hpGC, which is much higher than those fabricated with ammonia introduced during growth [10]. As shown in Fig. 5, the N 1*s* spectrum of the N-hpGC can be dominantly deconvoluted into pyridinic N (60.4%), pyrrolic N (23.7%), and quanternary N (9.9%). These nitrogen species together with topological defects are believed to serve as active sites for both ORR and OER.

3.3 Bifunctional ORR/OER performance of the hpGC

As-obtained hpGC and N-hpGC materials exhibit a hierarchical porous structure with micro-sized hollow cubes and mesopores on the wall, which is favorable for the heterogeneous electrocatalysis with easily accessible active sites [33]. Besides, the abundant pores and edges provide plentiful defect sites and nitrogen doping generates heteroatom active sites, resulting in considerable performance for bifunctional ORR and OER [34-37].

The ORR activity was evaluated by RRDE measurements in an O_2-saturated 0.10 M KOH. As presented in Fig. 6a, both hpGC and N-hpGC exhibit electrocatalytic activities for ORR, indicate the activity of the defect sites even without nitrogen doping [38-40]. The limiting current density for the N-hpGC (~5.28 mA cm^{-2}) is much larger than that for the hpGC (3.65 mA cm^{-2}), and the potential required for a current density of -3.0 mA cm^{-2} is positively shifted by 350 mV. Furthermore, the electron transfer number for the N-hpGC is also larger than that for the hpGC over the whole potential range from 0 to 0.6 V (Fig. 6b), suggesting a more favorable catalytic pathway. Additionally, the N-hpGC also delivers a significantly improved OER activity compared with the hpGC (Fig. 6c). Considering that they possess similar structure and porosity, the performance enhancement is ascribed to the

nitrogen doping, which has been widely demonstrated as the active origins in metal-free nanocarbon materials [41].

4 Conclusions

The SAPO-34 crystals were employed as the catalytic templates for graphene deposition. 3D hierarchical porous graphene cages can be facilely obtained via CVD of methane on SAPO-34 templates, with a precise replication of the morphology and ultrathin features. Nitrogen atoms are incorporated into the carbon matrix with a high doping level of 6.84 at% by the subsequent annealing under ammonia. Due to the unique porosity, abundant defects, and favorable doping, as-obtained N-hpGC exhibits considerable bifunctional activities for both ORR and OER. The SAPO-34 is expected to be a versatile platform for the study of the graphene growth on templates with different acidities. By tuning the structure of SAPO-34 or utilizing the nano-sized framework cages, the graphene material with optimized morphology or hybrid with confined metal nanoparticles (even single atom sites) can be obtained. Furthermore, this work inspires the utilization of industrial catalysts as the template for graphene growth, which may open a new window in materials science. It provides a new strategy to fabricate 3D porous and functionalized graphene materials with engineered structures and modified surface chemistry, aiming at promising applications in energy storage and conversion.

Acknowledgements

This work was supported by National Key Research and Development Program (2016YFA0200101), Natural Scientific Foundation of China (21422604), Beijing Municipal Commission of Science and Technology (Z161100002116019), and Tsinghua University Initiative Scientific Research Program.

References

[1] Zhu Y P, Guo C X, Zheng Y, et al. Surface and interface engineering of noble-metal-free electrocatalysts for efficient energy conversion processes [J]. Accounts of Chemical Research, 2017, 50: 915-923.

[2] Wang S, Jiang S P. Prospects of fuel cell technologies [J]. National Science Review, 2017, 4: 163-166.

[3] Zhang X Q, Cheng X B, Zhang Q. Nanostructured energy materials for electrochemical energy conversion and storage: A review [J]. Journal of Energy Chemistry, 2016, 25: 967-984.

[4] Tu Y C, Deng D H, Bao X H. Nanocarbons and their hybrids as catalysts for non-aqueous lithium-oxygen batteries [J]. Journal of Energy Chemistry, 2016, 25: 957-966.

[5] Yang H C, Liang J, Wang Z X, et al. Applications of porous carbon materials in the electrocatalysis of the oxygen reduction reaction [J]. New Carbon Materials, 2016, 31: 243-263.

[6] Zhu Q L, Xu Q. Immobilization of ultrafine metal nanoparticles to high-surface-area materials and their catalytic applications [J]. Chem, 2016, 1: 220-245.

[7] Yuan L Z, Yan Z, Jiang L H, et al. Gold-iridium bifunctional electrocatalyst for oxygen reduction and oxygen evolution reactions [J]. Journal of Energy Chemistry, 2016, 25: 805-810.

[8] Li B-Q, Tang C, Wang H-F, et al. An aqueous preoxidation method for monolithic perovskite electrocatalysts with enhanced water oxidation performance [J]. Science Advances, 2016, 2: e1600495.

[9] Li B-Q, Zhang S-Y, Tang C, et al. Anionic regulated nife (oxy)sulfide electrocatalysts for water oxidation [J]. Small, 2017, 13: 1700610.

[10] Wang H-F, Tang C, Zhang Q. Template growth of nitrogen-doped mesoporous graphene on metal oxides and its use as a metal-free bifunctional electrocatalyst for oxygen reduction and evolution reactions [J]. Catalysis Today, 2018, 301: 25-31.

[11] Tang C, Zhang Q. Nanocarbon for oxygen reduction electrocatalysis: Dopants, edges, and defects [J]. Advanced Materials, 2017, 29: 1604103.

[12] Wang L P, Jia W S, Liu X F, et al. Sulphur-doped ordered mesoporous carbon with enhanced electrocatalytic activity for the oxygen reduction reaction [J]. Journal of Energy Chemistry 2016, 25: 566-570.

[13] Seredych M, Laszlo K, Rodriguez-Castellon E, et al. S-doped carbon aerogels/GO composites as oxygen reduction catalysts [J]. Journal of Energy Chemistry, 2016, 25: 236-245.

[14] Tang C, Wang H S, Wang H F, et al. Spatially confined hybridization of nanometer-sized NiFe hydroxides into nitrogen-doped graphene frameworks leading to superior oxygen evolution reactivity [J]. Advanced Materials, 2015, 27: 4516-4522.

[15] Tang C, Wang H F, Zhu X L, et al. Advances in hybrid electrocatalysts for oxygen evolution reactions: Rational integration of nife layered double hydroxides and nanocarbon [J]. Particle & Particle Systems Characterization, 2016, 33: 473-486.

[16] Tang C, Titirici M-M, Zhang Q. A review of nanocarbons in energy electrocatalysis: Multifunctional substrates and highly active sites [J]. Journal of Energy Chemistry, 2017, 26: 1077-1093.

[17] Wang J, Wu Z X, Han L L, et al. Rational design of three-dimensional nitrogen and phosphorus co-doped graphene nanoribbons/cnts composite for the oxygen reduction [J]. Chinese Chemical Letters, 2016, 27: 597-601.

[18] Guo M Q, Huang J Q, Kong X Y, et al. Hydrothermal synthesis of porous phosphorus-doped carbon nanotubes and their use in the oxygen reduction reaction and lithium-sulfur batteries [J]. New Carbon Materials, 2016, 31: 352-362.

[19] Guo S J, Yang Y M, Liu N Y, et al. One-step synthesis of cobalt, nitrogen-codoped carbon as nonprecious bifunctional electrocatalyst for oxygen reduction and evolution reactions [J]. Science Bulletin, 2016, 61: 68-77.

[20] Li R N, Zhang D T, Zhou Y Y, et al. Synthesis and characterization of a novel binuclear iron phthalocyanine/reduced

graphene oxide nanocomposite for non-precious electrocatalyst for oxygen reduction [J]. Science China-Chemistry, 2016, 59: 746-751.

[21] Li Y R, Chen J, Huang L, et al. Highly compressible macroporous graphene monoliths via an improved hydrothermal process [J]. Advanced Materials, 2014, 26: 4789-4793.

[22] Chen Z P, Ren W C, Gao L B, et al. Three-dimensional flexible and conductive interconnected graphene networks grown by chemical vapour deposition [J]. Nature Materials, 2011, 10: 424-428.

[23] Tang C, Li B-Q, Zhang Q, et al. CaO-templated growth of hierarchical porous graphene for high-power lithium–sulfur battery applications [J]. Advanced Functional Materials, 2016, 26: 577-585.

[24] Zhao M-Q, Zhang Q, Huang J-Q, et al. Unstacked double-layer templated graphene for high-rate lithium-sulphur batteries [J]. Nature Communications, 2014, 5: 3410.

[25] Lv Y, Fang Y, Wu Z, et al. In-situ confined growth of monodisperse Pt nanoparticle@graphene nanobox composites as electrocatalytic nanoreactors [J]. Small, 2015, 11: 1003-1010.

[26] Cui Y, Zhang Q, He J, et al. Pore-structure-mediated hierarchical SAPO-34: Facile synthesis, tunable nanostructure, and catalysis applications for the conversion of dimethyl ether into olefins [J]. Particuology, 2013, 11: 468-474.

[27] Sun Q, Xie Z, Yu J. The state-of-the-art synthetic strategies for SAPO-34 zeolite catalysts in methanol-to-olefin conversion [J]. National Science Review 2017: doi: 10.1093/nsr/nwx103.

[28] Shi J L, Tang C, Peng H J, et al. 3D mesoporous graphene: CVD self-assembly on porous oxide templates and applications in high-stable Li-S batteries [J]. Small, 2015, 11: 5243-5252.

[29] Tian G L, Zhao M Q, Yu D S, et al. Nitrogen-doped graphene/carbon nanotube hybrids: In situ formation on bifunctional catalysts and their superior electrocatalytic activity for oxygen evolution/reduction reaction [J]. Small, 2014, 10: 2251-2259.

[30] Tang H L, Cai S C, Xie S L, et al. Metal-organic-framework-derived dual metal- and nitrogen-doped carbon as efficient and robust oxygen reduction reaction catalysts for microbial fuel cells [J]. Advanced Science, 2016, 3: 1500265.

[31] Hou T Z, Chen X, Peng H J, et al. Design principles for heteroatom-doped nanocarbon to achieve strong anchoring of polysulfides for lithium-sulfur batteries [J]. Small, 2016, 12: 3283-3291.

[32] Hou T Z, Xu W T, Chen X, et al. Lithium bond chemistry in lithium-sulfur batteries [J]. Angewandte Chemie-international Edition, 2017, 56: 8178-8182.

[33] Tian G L, Zhang Q, Zhang B S, et al. Toward full exposure of "active sites": Nanocarbon electrocatalyst with surface enriched nitrogen for superior oxygen reduction and evolution reactivity [J]. Advanced Functional Materials, 2014, 24: 5956-5961.

[34] Su F Y, Xie L J, Sun G H, et al. Theoretical research progress on the use of graphene in different electrochemical processes [J]. New Carbon Materials, 2016, 31: 363-377.

[35] Pan T, Liu H Y, Ren G Y, et al. Metal-free porous nitrogen-doped carbon nanotubes for enhanced oxygen reduction and evolution reactions [J]. Science Bulletin, 2016, 61: 889-896.

[36] Yan D, Li Y, Huo J, et al. Defect chemistry of nonprecious-metal electrocatalysts for oxygen reactions [J]. Advanced Materials, 2017, 29: 1606459.

[37] Wei L, Karahan H E, Zhai S L, et al. Microbe-derived carbon materials for electrical energy storage and conversion [J]. Journal of Energy Chemistry, 2016, 25: 191-198.

[38] Jiang Y, Yang L, Sun T, et al. Significant contribution of intrinsic carbon defects to oxygen reduction activity [J]. ACS Catalysis, 2015, 5: 6707-6712.

[39] Tang C, Wang H-F, Chen X, et al. Topological defects in metal-free nanocarbon for oxygen electrocatalysis [J]. Advanced Materials, 2016, 28: 6845-6851.

[40] Jia Y, Zhang L Z, Du A J, et al. Defect graphene as a trifunctional catalyst for electrochemical reactions [J]. Advanced Materials, 2016, 28: 9532-9538.

[41] Li M T, Zhang L P, Xu Q, et al. N-doped graphene as catalysts for oxygen reduction and oxygen evolution reactions: Theoretical considerations [J]. Journal of Catalysis, 2014, 314: 66-72.